A phase field study of morphological instabilities in multilayer thinfilms

B. G. Chirranjeevi [a] T. A. Abinandanan [*,b] M. P. Gururajan [c]

[a] *Department of Metallurgical and Materials Engineering, Indian Institute of Technology Madras, Chennai, India*

[b] *Department of Materials Engineering, Indian Institute of Science, Bangalore, India*

[c] *Department of Materials Science and Engineering, Northwestern University, Evanston, Illinois, USA*

Abstract

We study the microstructural evolution of multiple layers of elastically stiff films embedded in an elastically soft matrix using a phase field model. The coherent and planar film/matrix interfaces are rendered unstable by the elastic stresses due to a lattice parameter mismatch between the film and matrix phases, resulting in the break up of the films into particles. With an increasing volume fraction of the stiff phase, the elastic interactions between neighbouring layers lead to (a) interlayer correlations from an early stage, (b) a longer wavelength for the maximally growing wave, and therefore, (c) a delayed break-up; further, they promote a crossover in the mode of instability from a predominantly anti-symmetric (in-phase) one to a symmetric (out-of-phase) one. We have computed a stability diagram for the most probable mode of breakup in terms of elastic modulus mismatch and volume fraction. We rationalize our results in terms of the initial driving force for destabi-

lization, and corroborate our conclusions using simulations in elastically anisotropic systems.

Key words:
Phase field modelling, thin films, Asaro-Tiller-Grinfeld instability, microstructural evolution, elastically stressed solids
PACS: 46.15.-x, 46.32.+x, 68.65.Ac

1 Introduction

It is well known that the planar interface of a non-hydrostatically stressed solid in equilibrium with its melt or vapour is unstable with respect to perturbations [1–3]: this instability is known as Asaro-Tiller-Grinfeld (ATG) instability. Based on elastic and interfacial energy considerations alone, Grinfeld showed that in the absence of an interfacial energy, a planar boundary between a solid and its melt or vapour is unstable with respect to perturbations of any wavelength; the interfacial energy sets the lower wavelength limit of this instability [4].

The literature on ATG instabilities is vast and varied to be summarized here; we refer the interested reader to the excellent monographs of Nozières (chapter 1 of [5]), Pimpinelli and Villain [6], and Freund and Suresh [7], and the reviews (and references therein) of Shchukin and Bimberg [8], Gao and Nix [9], Stangl et al [10], Johnson and Voorhees [11] and Balibar et al [12] for a summary of the experimental and theoretical studies.

* Corresponding author
Email address: abinandanan@gmail.com (T. A. Abinandanan).

Sridhar et al [13,14] (hereafter, referred to as SRS) have shown the crucial role played by an elastic modulus mismatch in promoting ATG instabilities; more specifically, for a misfitting thin film layer embedded in a matrix (both in the presence and absence of externally applied stresses), the planar film/matrix interface is unstable with respect to perturbations as long as the film is elastically stiffer than the matrix. In the case of a non-misfitting film embedded in a matrix under an externally applied stress, the interface is unstable as long as the film and matrix have different elastic constants.

Using a linear stability analysis that accounts for both curvature (or interfacial) and elastic contributions, SRS identify two dominant modes of instabilities that a film/matrix interface can undergo. Depending on whether the undulations of the upper and lower interfaces of a film are out of phase or in phase (see their schematic in Fig. 8 of [14]), these modes are known as symmetric and anti-symmetric, respectively. In addition, their stability diagrams show that the anti-symmetric mode is promoted at higher values of the driving force for film destabilization.

While a linear stability analysis is ideal for the study of onset of instability, it can not accurately predict the evolution, break up and coarsening of the microstructure. Further, for multilayer films, interlayer correlations are far too complicated to be included in such an analysis; thus, for example, the multilayer part of the study by SRS has been carried out for a particular kind of interlayer correlation in which the undulations of the upper interfaces of all the films are in phase.

There are several simulation studies on the elastic stress induced morphological instabilities in thin films [15–35]; while most of these studies are based on the

phase field method [15–27], the rest are based on the phase field crystal [28,29], continuum, sharp-interface [30–33], and, atomistic [34,35] models.

All phase field studies that we are aware of are for the evolution of multilayer films in the presence of the film/vapour (or film/melt) interface. In these studies, the microstructural evolution is influenced by both the multilayer setting and the film/vapour interface, leading to different behaviours of individual layers depending on their distance from the film/vapour interface. Our study, on the other hand, focuses on a 'pure' multilayer geometry. It allows us to determine the effects that arise from the multilayers alone. It also allows us to explore quantitatively the role of system parameters in determining the mode of onset of instability and the maximally unstable wavelength.

This paper is organized as follows: we present a brief outline of the formulation in Section 2; in Section 3, we present our numerical simulation results and discuss the key features of multilayer evolution in Section 4; we conclude the paper with a short summary.

2 Formulation

In this section, we outline our phase field model for systems that are elastically inhomogeneous and anisotropic. The model is based on the Cahn-Hilliard equation [36], and details of its formulation and numerical implementation may be found in Ref. [37,38].

We consider a binary alloy consisting of two phases, namely, p and m, whose scaled equilibrium compositions in the absence of elastic stresses are unity and zero, respectively. Our phase field formulation starts with the following

expression for the total free energy F of a system with spatial variations in composition c:

$$F = N_v \int [Ac^2(1-c)^2 + \kappa(\nabla c)^2] dV + \frac{1}{2} \int \sigma^{el} : \epsilon^{el} dV, \tag{1}$$

where N_v is the number of atoms per unit volume, κ is the (positive) gradient energy coefficient, A is the free energy barrier between the two phases, ϵ^{el} and σ^{el} are the elastic strain and stress fields, respectively, and ':' denotes tensor inner product. The microstructural evolution in the system is described by the Cahn-Hilliard equation:

$$\frac{\partial c}{\partial t} = \nabla \cdot M \nabla \mu, \tag{2}$$

where μ is the chemical potential, defined as the variational derivative of the free energy with respect to composition:

$$\mu = \frac{\delta (F/N_v)}{\delta c}. \tag{3}$$

The stress, σ^{el}, is obtained by assuming Hooke's law (that is, the phases m and p are linear elastic):

$$\sigma_{ij}^{el} = C_{ijkl} \epsilon_{kl}^{el}, \tag{4}$$

where we have used Einstein's convention of summation over repeated indices. C_{ijkl} is the elastic modulus tensor, and ϵ_{ij}^{el} is the elastic strain, given by

$$\epsilon_{ij}^{el} = \epsilon_{ij} - \epsilon_{ij}^{0}, \tag{5}$$

where ϵ_{ij}^{0} is the eigenstrain, and ϵ_{ij} is the total strain compatible with the displacement u_i:

$$\epsilon_{ij} = \frac{1}{2} \left(\frac{\partial u_i}{\partial r_j} + \frac{\partial u_j}{\partial r_i} \right). \tag{6}$$

The displacement field is obtained by solving the equation of mechanical equilibrium

$$\frac{\partial \sigma_{ij}^{el}}{\partial r_j} = 0. \tag{7}$$

We assume the following composition dependences for the elastic moduli and the eigenstrain:

$$C_{ijkl}(c) = C_{ijkl}^{eff} + \alpha(c)\Delta C_{ijkl}; \tag{8}$$

$$\epsilon_{ij}^{0}(c) = \beta(c)\epsilon^{T}\delta_{ij} \tag{9}$$

where $\alpha(c)$ and $\beta(c)$ are scalar interpolating functions of composition, $C_{ijkl}^{eff} = (C_{ijkl}^{p} + C_{ijkl}^{m})/2$ is the arithmetic average of the elastic moduli of the two phases, $\Delta C_{ijkl} = C_{ijkl}^{p} - C_{ijkl}^{m}$ is the difference between the elastic modulus of the p phase and that of m phase, ϵ^{T} denotes the strength of the eigenstrain and δ_{ij} is the Kronecker Delta.

2.1 Simulation details and parameters

We use a semi-implicit Fourier spectral technique to solve the evolution equation for composition Eq. 2 in two dimensions (2D), with periodic boundary conditions. The evaluation of the right hand side (RHS) of Eq. 2 involves not only the composition and its gradient but also the elastic stress and strain fields. For a given composition field, we obtain the elastic stress and strain fields by solving the equation of mechanical equilibrium (Eq. 7). The solution of the equation of mechanical equilibrium is also obtained using a Fourier based iterative technique, assuming prescribed displacement conditions (in other words, the homogeneous strain is zero); see [37–39] for details. Once we obtain the stress and strain fields, the RHS of Eq. 2 can be evaluated, which is then used for time stepping and hence, for following the microstructural evo-

lution. All the (discrete) Fourier transforms needed for our simulations were carried out using the freeware FFTW developed by Frigo and Johnson [40].

All our simulations are carried out using a non-dimensional version of Eq. 2, wherein the non-dimensional values of κ, A and M are unity. For cubic elastic elastic constants, circular averages of the three Voigt constants, $\overline{C_{11}}$, $\overline{C_{12}}$, and $\overline{C_{44}}$, are used to define the shear modulus G, Poisson's ratio ν, and the Zener anisotropy parameter A_Z [41]:

$$G = \overline{C_{44}}, \tag{10}$$

$$\nu = \frac{1}{2}\frac{\overline{C_{12}}}{\overline{C_{12}} + \overline{C_{44}}}, \tag{11}$$

and,

$$A_Z = \frac{2\overline{C_{44}}}{\overline{C_{11}} - \overline{C_{22}}} \tag{12}$$

Further, we also assume $A_Z^m = A_Z^p$ and $\nu^m = \nu^p$. Thus, a complete description of the system's elastic paramters requires specifying the values of A_Z^m, ν^m, and G^m, along with the inhomogeneity parameter δ, defined as the ratio of the shear moduli the p and m phases: $\delta = G^p/G^m$. We have used $\nu = 0.3$, and $G^m = 50$; we have assumed (except in Fig. 7) elastic isotropy: $A_Z = 1$. For the interpolation function for eigenstrain, we have used $\beta = c^3(1 - 15c + 6c^2)$; this implies that the unstressed m phase is used as the reference state. For the interpolation function for elastic moduli, we use: $\alpha = c^3(1 - 15c + 6c^2) - 1/2$.

All our simulations are on two dimensional systems, and use a spatial grid of $\Delta x = \Delta y = 1$. The non-dimensionalized Cahn-Hilliard parameters are: $A = 1$, $\kappa = 1$, and $M = 1$. For time stepping, we use $\Delta t = 0.5$ for the first 10000 time steps and $\Delta t = 1.0$ for the rest of the evolution.

3 Results

Our simulations start with a system with alternating layers of p and m phases, with an equal interlayer spacing of H. Their thicknesses are h and $(H - h)$, and compositions are 1.0 and 0.01, respectively. We use periodic boundary conditions, and the microstructure evolves under zero homogeneous strain. Since the unstressed matrix is the reference state with respect to which strains are measured, and since the p (film) phase has a larger lattice parameter than the matrix, the elastically stiff p layers are under a compressive stress, causing their instability.

After a short simulation run (upto, say, $t = 500$), the microstructure exhibits diffuse interfaces. The reported values of h, the thickness of p-phase films, is obtained from this microstructure. Since all the p-phase films have the same thickness h (defined as the thickness of the p layer with a composition of over 0.5), its volume fraction is $f = h/H$. [We note that the average composition c_o is not an accurate measure of volume fraction of the p phase, because the elastic stresses shift the equilibrium compositions of the two phases.]

3.1 A single layer film embedded in a matrix

Fig. 1 shows the stress-driven evolution of a single thin film embedded in a matrix; due to periodic boundary conditions, the film is not isolated; the volume fraction, however, is small: $(h/H) = 0.043$. Fig. 1(a) shows a film with $\delta = 2$ and $h = 11$, while Fig. 1(b) is for a stiffer and thicker film: $\delta = 4$, $h = 22$. While the mode of instability in the former is symmetric (i.e., the undulations on the upper and lower interfaces of the film are out of phase by

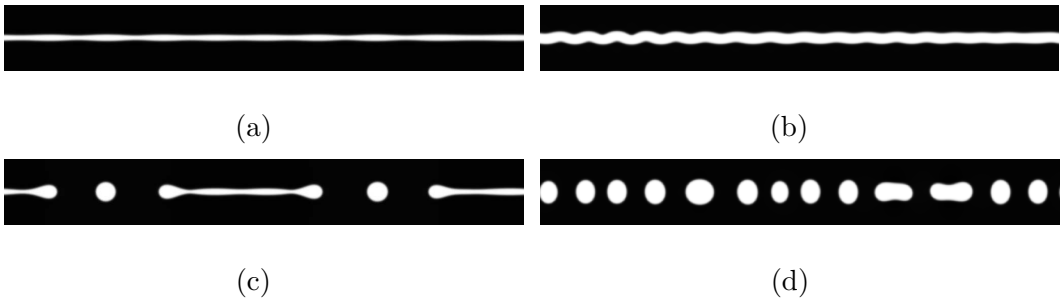

Fig. 1. Microstructural development in a single stiff layer embedded in a soft matrix. The left and right columns represent, respectively, low and high driving force for film destabilization, and the top and bottom rows are for, respectively, onset of instability and well after film break-up. Left column: $\delta = 2$, $h = 11$, (a) $t = 1.28 \times 10^5$ and (c) $t = 1.44 \times 10^5$. Right column: $\delta = 4$, $h = 22$, (b) $t = 2.0 \times 10^4$, and (d) $t = 3.5 \times 10^4$.

half a wavelength), that in the thicker and stiffer film is anti-symmetric (i.e., the undulations on the upper and lower interfaces are in phase). Further, the wavelength of the undulations is higher, and the time taken for break-up is longer, for the symmetric system.

The transition from a symmetric mode for the onset of instability in Fig. 1(a) to an anti-symmetric one in Fig. 1(b) is in agreement with the results of SRS, who also found such a transition with an increasing driving force for film destabilization (i.e., with increasing δ and h). Further, the maximally unstable wavelength $\lambda_{max} \approx 102$ observed in the simulations of the symmetric instability mode (Fig. 1(a)) are in agreement with the value of 80 obtained from a linear stability analysis (similar to that of Sridhar et al [14]) for film evolution under volume diffusion control; the details of the analysis can be found at [42].

A larger driving force for film destabilization (due to larger values of h and δ) also leads to a smaller value of the maximally growing wavelength ($\lambda_{max} \approx 60$) and time for break-up ($t \approx 33000$) observed in the anti-symmetric case, as

compared to $\lambda_{max} \approx 102$ and $t \approx 140000$ in the symmetric case.

3.2 Multilayer thin film assemblies

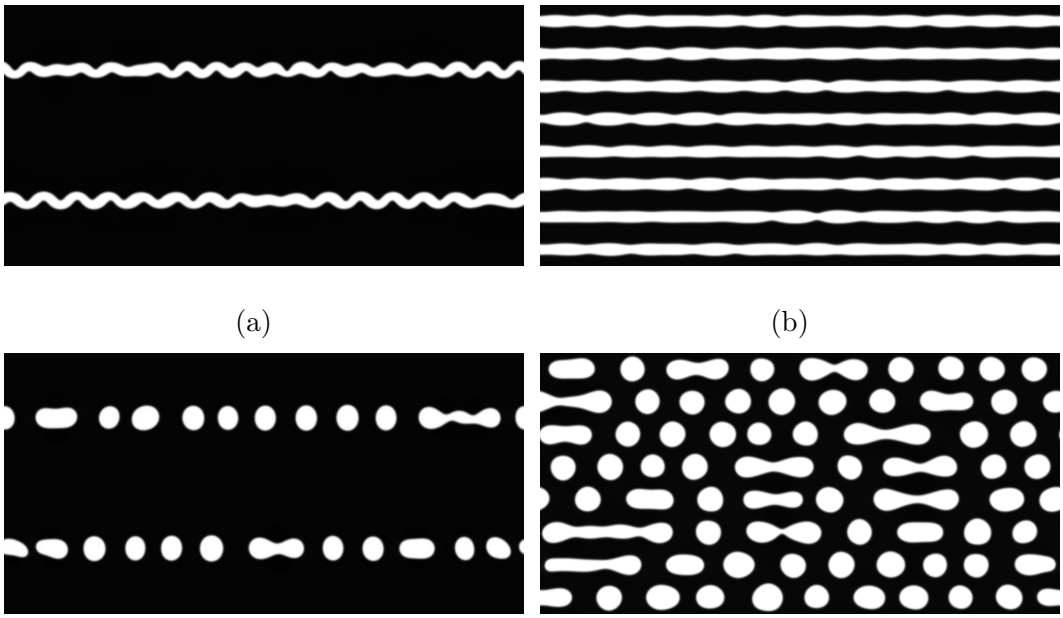

Fig. 2. Evolution of multilayers with $\delta = 4$ at two different volume fractions. Left column: $f = 0.086$, two layers in the simulation cell,, (a) $t = 25000$ and (c) $t = 36000$. Right column: $f = 0.34$, eight layers in the simulation cell, (b) $t = 36000$ and (d) $t = 49000$.

Fig. 2 shows the microstructural evolution in systems with volume fractions of $f = 0.086$ (left column) and $f = 0.34$ (right column); they correspond to two and eight layers, respectively, of the stiffer film (with $h = 22$ each) stacked in a 1024×512 simulation cell. The top row shows the onset of instability in these two systems, while the bottom row shows an advanced stage of film break up.

There are two key differences in the microstructural evolution of the two systems in Fig. 2. The onset of instability is anti-symmetric in the system with

two layers, while it is symmetric in that with eight layers. Further, the maximally unstable wavelength is higher (and the time for break up is longer), in the eight layer case as compared to the two layer case.

3.2.1 Height-height correlations

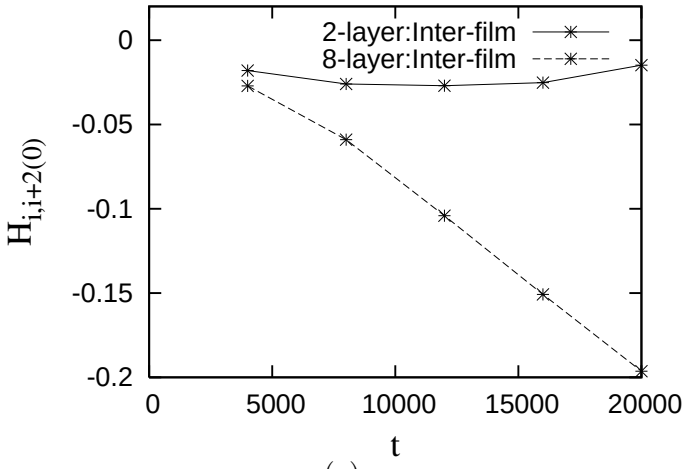

(a)

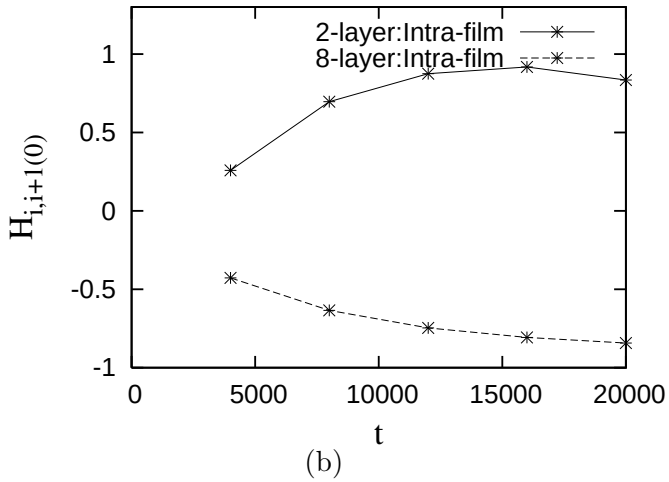

(b)

Fig. 3. Development of (a) inter-layer and (b) intra-layer correlations with time for two layers ($f = 0.086$) and eight layers ($f = 0.36$) in a 1024×512 simulation cell. The lines joining the data points are only a guide to the eye. $\delta = 4$, $h = 22$.

A closer examination of Fig. 2(d) reveals that the broken-up particles of the film phase show a high degree of correlation across layers: particles in a given

layer appear, on average, in the middle of two particles in its two adjacent layers. On the other hand, in the 2-layer case, such correlations do not appear significant. These correlations can be more quantitatively studied using the height-to-height correlations, obtained from a procedure described in the Appendix. Of special importance to us is the behaviour of $\mathcal{H}(0)$, the time evolution of which is shown in Figs. 3(a) and 3(b), respectively, for inter-layer and intra-layer correlations.

Fig. 3(a) depicts the time dependence of inter-layer correlations $\mathcal{H}_{i,i+2}(0)$ for the 2-layer and 8-layer systems. These correlations are small (and negative) at $t = 4000$ in both the systems; however, they stay small in the 2-layer case, while they grow stronger with time in the 8-layer case. In particular, in the 8-layer system, the top (or bottom) interfaces of adjacent layers develop a negative correlation (i.e., their undulations are out of phase). Interestingly, the correlations are significant even at $t = 10,000$, when the interface undulations are barely discernible. Since each film in the 8-layer case, in Fig. 2(b), undergoes a symmetric instability creating alternating bulges and necks, the negative value for the inter-layer correlation $\mathcal{H}_{i,i+2}(0)$ implies that the bulges in any given layer are aligned (along the y-direction) with the necks of the adjacent layers, and vice versa. Further evolution of this correlated undulations leads to the final (fully broken-up) microstructure, shown in Fig. 2(d), which is also highly correlated.

Finally, Fig. 3(b) for intra-layer correlations confirms our observations about the instability mode: in phase or out of phase. In the two layer case, the onset is anti-symmetric or in-phase ($\mathcal{H}_{i,i+1}(0) > 0$); with increasing time, this correlation becomes stronger. Similarly, for the eight layer case, we find $\mathcal{H}_{i,i+1}(0) < 0$, indicating that the onset is symmetric or out-of-phase.

3.2.2 Effect of volume fraction and inhomogeneity

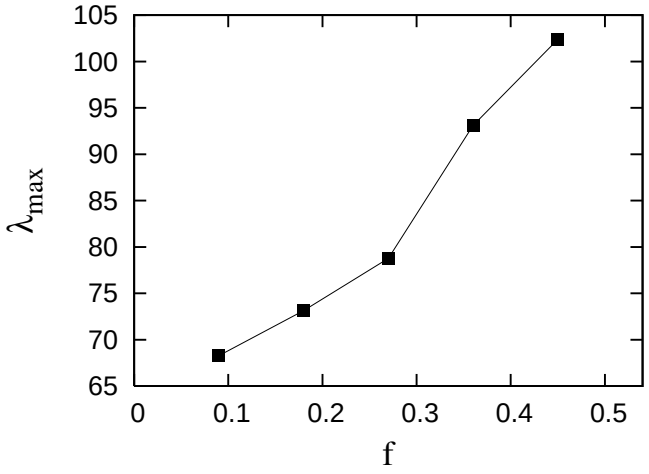

Fig. 4. Variation of the maximally unstable wavelength λ_{max} with volume fraction f of the (stiffer) film phase in systems with $\delta = 4$ and $h = 22$. The line joining the data points is only a guide to the eye.

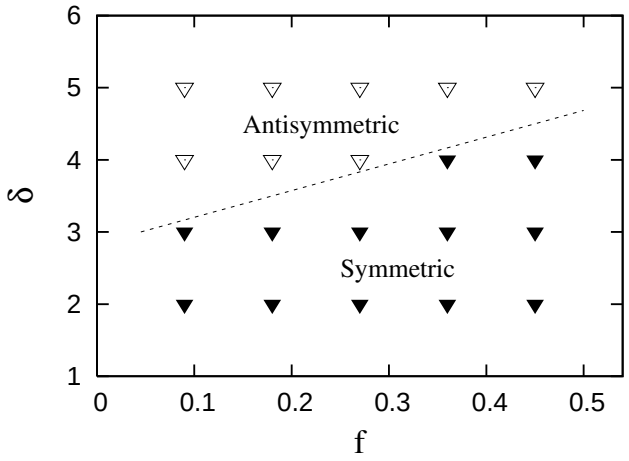

Fig. 5. Stability diagram depicting the most likely instability mode in terms of volume fraction f of the stiffer phase and the inhomogeneity ratio δ in systems with $h = 22$. The dashed line is only a guide to the eye.

As noted in Section. 3.2 above, for a given inhomogeneity δ the maximally growing wavelength of the instability λ_{max} increases with increasing volume fraction f of the film phase. In Fig. 4, we show this trend using the data for five different volume fractions.

We summarize the role of volume fraction and elastic inhomogeneity using

an instability mode diagram in Fig. 5. This figure shows that, for a given volume fraction, increasing δ makes the system switch from a symmetric to an anti-symmetric mode. On the other hand, for a given δ, increasing volume fraction leads to a reverse switch, namely, from an anti-symmetric mode to a symmetric one.

3.2.3 Effect of film thickness

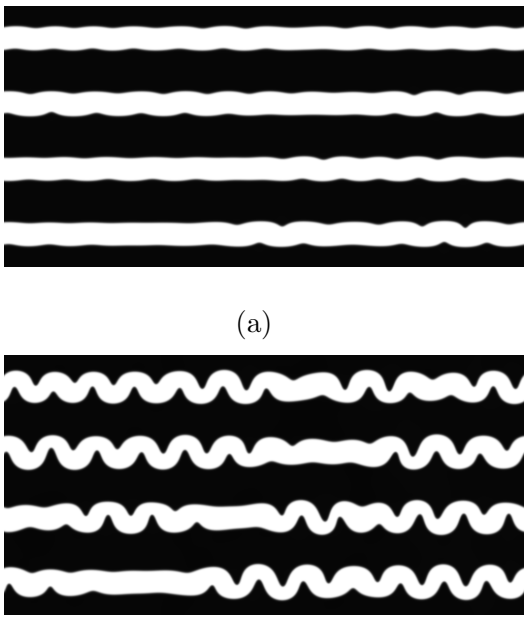

(a)

(b)

Fig. 6. Multilayer microstructures at (a) $t = 49000$ and (b) $t = 59000$ for a thin film assembly with $\delta = 4$, $f = 0.35$ and $h = 45$. The film thickness is double (but the volume fraction f is nearly the same as) that in Fig. 2(b) and (d).

For a given volume fraction, increasing the film height increases the driving force for destabilizing the film, as does increasing the elastic inhomogeneity δ. Since Fig. 5 shows that an increasing δ promotes an anti-symmetric onset, we expect an increasing h to do the same. Thus, in the system with $f = 0.34$, for example, increasing h from 22 to 45 (while keeping the volume fraction $f = h/H$ the same) does indeed lead to an anti-symmetric break-up; see

Fig. 6.

3.2.4 Effect of anisotropy

In addition to tuning the film thickness h and inhomogeneity δ, there is yet another way of changing the driving force for film destabilization if we consider elastically anisotropic systems: in such systems, if the films have an elastically unfavourable (favourable) orientation, this driving force is increased (decreased).

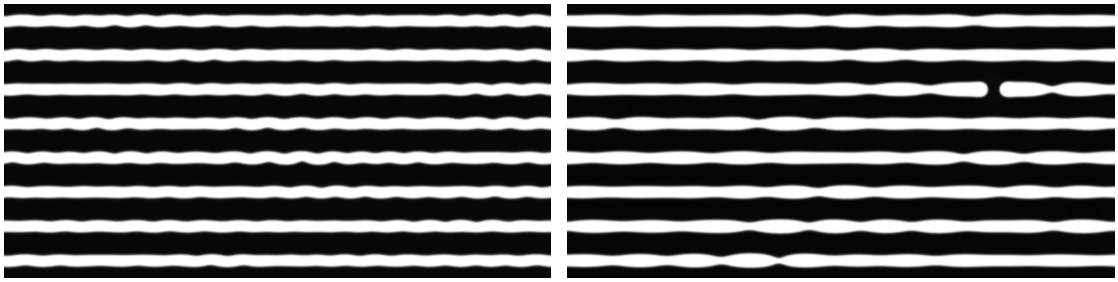

(a) (b)

Fig. 7. Multilayer evolution at (a) $t = 16000$ and (b) $t = 64000$ in elastically aniostropic systems: $A_Z = 0.8$ and $A_Z = 1.2$, respectively. All the other parameters ($\delta = 4$, $f = 0.34$, $h = 22$, simulation cell: 1024×512) are the same as in Fig. 2(b) for an elastically isotropic ($A_Z = 1$) system.

Consider a system with a Zener anisotropy parameter of $A_Z = 0.8$; the $\langle 10 \rangle$ directions are elastically stiffer than the $\langle 11 \rangle$ directions. Therefore, a film initially oriented along the [10]-direction (x axis) is in an elastically unfavourable geometry, and may be expected (based on Fig. 2) to exhibit an anti-symmetric instability mode. Fig. 7(a) shows that this is indeed the case. By the same argument, a film oriented along [10]-direction in a system with $A_Z = 1.2$ would be expected to retain its symmetric instability mode; this, again, is shown to be true in Fig. 7(b). Finally, the behaviour of the maximally unstable wave-

length in these simulations is also consistent with these arguments: for the same film thickness of $h = 20$, and as compared with the elastically isotropic system, an anisotropy of $A_Z = 0.8$ leads to lower λ_{max} while an anisotropy of $A_Z = 1.2$ leads to a higher λ_{max}; see Table 1.

Table 1

Variation of λ_{max} with h and A_Z

h	A_Z	λ_{max}	Mode
22	1.0	93	Symmetric
45	1.0	85	Antisymmetric
22	1.2	128	Symmetric
22	0.8	64	Antisymmetric

4 Discussion

An important conclusion from our simulation study is that, in a system with a given combination of interfacial energy γ, elastic inhomogeneity ratio δ and film height h, an increase in volume fraction (or, equivalently, a decrease in layer spacing) may (a) change the onset of instability from an anti-symmetric mode to a symmetric one, (b) increase the wavelength of the maximally unstable perturbation, and (c) induce inter-layer correlation. A related finding is the development of inter-layer correlations when the perturbations of film-matrix interface are barely discernible.

It is convenient to examine the early stages of evolution of the multilayer

microstructure using energy arguments. The elastic energy in the system is the primary destabilizing factor, while the interfacial energy is the stabilizing factor. The work of SRS has established that their effects are described adequately through the two factors δ and $\theta = \gamma / \left[E_A h (\epsilon^T)^2\right]$. SRS also established that an increase in elastic energy (through an increase in δ or a decrease in θ) leads to a change in the onset of instability from a symmetric (out of phase) mode to an anti-symmetric (in phase) mode.

Our results show that in a multilayer setting, volume fraction (or, equivalently, the layer spacing) is an independent factor with an influence on film instability. Clearly, a decrease in layer spacing leads to greater elastic interactions among the layers; our results indicate that the primary effect of these elastic interactions is to reduce the driving force for destabilizing the films. Thus, for example, the dominant wavelength is higher, and the instability mode may even become symmetric. This explanation is further strengthened by other evidence from our study: starting from a high volume fraction where the symmetric mode is dominant, anti-symmetric mode can be obtained again through a change in system parameters whose primary effect is to increase the driving force for film destabilization: an increase in δ or h, or an elastic anisotropy that makes the original film orientation unfavourable.

While the development of inter-layer correlations is an expected result, their early development is somewhat surprising, because they start to appear at a stage when the perturbations on the film-matrix interface are barely discernible. These inter-layer correlations $\mathcal{H}_{i,i+2}(0)$ may be positive or negative. For example, in the isotropic system with a symmetric instability mode, $\mathcal{H}_{i,i+2}(0) < 0$ (i.e., bulges in one film are aligned with the necks in the neighbouring films). However, in the anisotropic system with $A_Z = 0.8$, where the

instability mode is anti-symmetric, $\mathcal{H}_{i,i+2} > 0$; i.e., the hills (valleys) on one film are aligned with its neighbour's hills (valleys).

As pointed out in Section 1, the possibility of inter-layer correlations renders a linear stability analysis of multilayer systems impossible except for specific correlations. For example, the multilayers studied by SRS assumed a particular correlation among the layers; as it turns out, this correlation, in which the bulges in adjacent layers are aligned, is not the one that is observed (see Fig. 2(a)).

5 Conclusions

Instability in stressed multilayers has been studied using phase field simulations of systems in which the film-matrix misfit is the only source of stress. Our study shows that, in addition to the elastic inhomogeneity and film thickness, the volume fraction is another important factor that controls the mode of instability. In particular, an increase in volume fraction increases the wavelength of the maximally unstable perturbation, leads to correlations in interface perturbations in neighbouring layers. It also promotes a transition in the mode of instability from an anti-symmetric mode to a symmetric one.

Appendix

Consider a microstructure consisting of M_f uniformly spaced films of the p phase embedded in a matrix. Thus, there are $2M_f$ film-matrix interfaces. With respect to the stiffer film phase, an i-th interface is designated as bottom when

i is odd, and top when i is even.

For each interface i, we define a height function $y_i(x)$ as the y-coordinate corresponding to $c = 0.5$. Let $\overline{y_i}$ and Σ_i be, respectively, the mean and standard deviation of this function. Thus, the function $Y_i(x)$, defined as

$$Y_i(x) = \frac{y_i(x) - \overline{y}_i}{\Sigma}$$

denotes the normalized undulations of the i-th interface about its mean position.

We define the height-to-height correlations $\mathcal{H}_{i,j}(z)$ between two interfaces i and j by the following integral:

$$\mathcal{H}_{i,j}(z) = \int Y_i^*(x) Y_j(z + x) dx,$$

With this definition, $\mathcal{H}_{i,j}(0)$ has the following interpretation: if it is positive (negative), undulations i and j are in phase (out of phase). For odd i, $\mathcal{H}_{i,i+1}(0)$ represents intra-layer correlations. On the other hand, for all i, $\mathcal{H}_{i,i+2}$ represents interlayer correlations.

Note that by using the Weiner-Kinchin theorem (p. 456 of [43]), the correlation integrals can be computed with ease in the Fourier space. Using $\tilde{Y}$ to represent the Fourier transform of Y, and $\tilde{Y}^*$ to represent the complex conjugate of $\tilde{Y}$, we have

$$\tilde{\mathcal{H}}_{i,j}(k) = \tilde{Y}_i^*(k) \tilde{Y}_j(k)$$

An inverse Fourier transform of $\tilde{\mathcal{H}}_{i,j}(k)$ yields $\mathcal{H}_{i,j}(z)$ in real space.

The inter-layer correlation $\mathcal{H}_{i,i+2}(0)$ and intra-layer correlation $\mathcal{H}_{i,i+1}(0)$ reported in Section 3 are averages over three independent simulations.

References

[1] R J Asaro and W A Tiller. Interface development during stress corrosion cracking. *Metallurgical Transactions A*, 3:1789–1796, 1972.

[2] M A Grinfeld. Instability of interface between non-hydrostatically stressed elastic body and melts. *Soviet Physics-Doklady*, 290:1358–1363, 1986.

[3] D J Srolovitz. On the stability of surfaces of stressed solids. *Acta Metallurgica*, 37:621–625, 1989.

[4] M A Grinfeld. The stress driven instability in elastic crystals: Mathematical models and physical manifestations. *Journal of Nonlinear Science*, 3:35–83, 1993.

[5] C Godrèche. *Solids far from equilibrium*. Cambridge University Press, Cambridge, UK, 1992.

[6] A Pimpinelli and J Villain. *Physics of crystal growth*. Cambridge University Press, Cambridge, UK, 1998.

[7] L B Freund and S Suresh. *Thin Film Materials: Stress, Defect Formation and Surface Evolution*. Cambridge University Press, Cambridge, UK, 2004.

[8] V A Shchukin and D Bimberg. Spontaneous ordering of nanostructures on crystal surfaces. *Reviews of Modern Physics*, 71:1125–1171, 1999.

[9] H Gao and W D Nix. Surface roughening of heteroepitaxial thin films. *Annual Reviews of Materials Science*, 29:173–209, 1999.

[10] J Stangl, V Holý, and G Bauer. Structural properties of self-organized semiconductor nanostructures. *Reviews of Modern Physics*, 76:725–783, 2004.

[11] P W Voorhees and W C Johnson. *The thermodynamics of elastically stressed crystals*, volume 59 of *Solid state physics: advances in research and applications*,

pages 1–201. Elsevier Academic Press, 2004.

[12] S Balibar, H Alles, and A Y Parshin. The surface of helium crystals. *Reviews of Modern Physics*, 77:317–370, 2005.

[13] N Sridhar, J M Rickman, and D J Srolovitz. Multilayer film stability. *Journal of Applied Physics*, 82:4582–4589, 1997.

[14] N Sridhar, J M Rickman, and D J Srolovitz. Microstructural stability of stressed lamellar and fiber composites. *Acta Metallurgica*, 45:2715–2733, 1997.

[15] J Müller and M Grant. Model of surface instabilities induced by stress. *Physical Review Letters*, 82:1736–1739, 1999.

[16] K Kassner and C Misbah. A phase-field approach for stress-induced instabilities. *Europhyscs Letters*, 46(2):217–223, 1999.

[17] K Kassner, C Misbah, J Müller, J Kappey, and P Kohlert. Phase-field modeling of stress-induced instabilities. *Physical Review E*, 63:036117 :1–27, 2001.

[18] M Haataja, J Müller, A D Rutenberg, and M Grant. Dynamics of dislocations and surface instabilities in misfitting heteroepitaxial films. *Physical Review B*, 65:035401: 1–5, 2001.

[19] J J Eggleston and P W Voorhees. Ordered growth of nanocrystals via a morphological instability. *Appled Physics Letters*, 80:306–208, 2002.

[20] M Haataja, J Müller, A D Rutenberg, and M Grant. Dislocations and morphological instabilities: continuum modeling of misfitting heteroepitaxial films. *Physical Review B*, 65:165414: 1–20, 2002.

[21] Y U Wang, Y M Jin, and A G Khachaturyan. Phase field microelasticity modeling of surface instability of heteroepitaxial thin films. *Acta Materialia*, 52:81–92, 2004.

[22] J Paret. Long-time dynamics of the three-dimensional biaxial Grinfeld instability. *Physical Review E*, 72:011105: 1–5, 2005.

[23] D J Seol, S Y Hu, Z K Liu, L Q Chen, S G Kim, and K H Oh. Phase-field modeling of stress-induced surface instabilities in heteroepitaxial thin films. *Journal of Applied Physics*, 98:044910 1–5, 2005.

[24] Y Ni, L H He, and A K Soh. Three-dimensional phase field simulation for surface roughening of heteroepitaxial films with elastic anisotropy. *Journal of Crystal Growth*, 284:281–292, 2005.

[25] S M Wise, J S Lowengrub, J S Kim, K Thornton, P W Voorhees, and W C Johnson. Quantum dot formation on a strain-patterned epitaxial thin film. *Applied Physics Letters*, 87:1–3, 2005.

[26] D -H Yeon, P -R Cha, and M Grant. Phase field model of stress-induced surface instabilities: Surface diffusion. *Acta Materialia*, 54:1623–1630, 2006.

[27] A Rätz, A Ribalta, and A Voigt. Surface evolution of elastically stressed films under deposition by a diffuse interface model. *Journal of Computational Physics*, 214:187–208, 2006.

[28] K R Elder and M Grant. Modeling elastic and plastic deformations in nonequilibrium processing using phase field crystals. *Physical Review E*, 70:051605: 1–18, 2004.

[29] K R Elder, N Provatas, J Berry, P Stefanovic, and M Grant. Phase-field crystal modeling and classical density functional theory of freezing. *Physical Review B*, 75:064107: 1–14, 2007.

[30] Y W Zhang. Self-organization, shape transition, and stability of epitaxially strained islands. *Physical Review B*, 61(15):10388–10392, 2000.

[31] Y W Zhang and A F Bower. Three-dimensional analysis of shape transitions

in strained-heteroepitaxial islands. *Applied Physics Letters*, 78(18):2706–2708, 2001.

[32] P Liu, Y W Zhang, and C Lu. Coarsening kinetics of heteroepitaxial islands in nucleationless Stranski-Krastanov growth. *Physical Review B*, 68:1–8, 2003.

[33] A Ramasubramaniam and V B Shenoy. Three-dimensional simulations of self-assembly of hut-shaped Si-Ge quantum dots. *Journal of Applied Physics*, 95(12):7813–7824, 2004.

[34] L Dong, J Schnitker, R W Smith, and D J Srolovitz. Stress relaxation and misfit dislocation nucleation in the growth of misfitting films: a molecular dynamics simulation study. *Journal of Applied Physics*, 83(1):217–227, 1998.

[35] C H Lam, C K Lee, and L M Sander. Competing roughening mechanisms in strained heteroepitaxy: a fast kinetic Monte Carlo study. *Physical Review Letters*, 89(21):216102: 1–4, 2002.

[36] J W Cahn and J E Hilliard. Free energy of a nonuniform system I. Interfacial free energy. *Journal of Chemical Physics*, 28:258–267, 1958.

[37] M P Gururajan and T A Abinandanan. A phase field study of microstructural evolution in elastically inhomogeneous systems. In J M Howe, D E Laughlin, J K Lee, U Dahmen, and W A Soffa, editors, *Proceedings of solid-solid phase transformations in inorganic materials*. TMS (The Minerals, Metals & Materials Society), 2005.

[38] M P Gururajan and T A Abinandanan. Phase field study of precipitate rafting under a uniaxial stress. *Acta Materialia*, 55:5015–5026, 2007.

[39] Y Hu and L Q Chen. A phase field model for evolving microstructures with strong elastic inhomogeneity. *Acta Materialia*, 49:1879–1890, 2001.

[40] M Frigo and S G Johnson. The design and implementation of FFTW3. *Proceedings of the IEEE*, 93:216–231, 2005.

[41] I Schmidt and D Gross. Directional coarsening in Ni-base superalloys: analytical results for an elasticity based model. *Proceedings of Royal Society (London)*, 455:3085–3016, 1999.

[42] M P Gururajan and T A Abinandanan. A linear stability analysis of ATG-instabilities in thin film assemblies under volume diffusion control. Unpublished notes. Available for download at http://www.imechanica.org/node/2703.

[43] K F Riley, M P Hobson, and S J Bence. *Mathematical methods for physics and engineering*. Cambridge University Press, Cambridge, UK, second edition, 2002.